Excited-State Diproton Transfer in [2,2′-Bipyridyl]-3,3′-diol: the Mechanism Is Sequential, Not Concerted

Felix Plasser,[†] Mario Barbatti,[†] Adélia J. A. Aquino,[†] and Hans Lischka*[,†,‡]

Institute for Theoretical Chemistry, University of Vienna, Waehringerstrasse 17, 1090 Vienna, Austria, and Institute of Organic Chemistry and Biochemistry, Academy of Sciences of the Czech Republic, Flemingovo nam. 2, CZ-16610 Prague 6, Czech Republic

Received: April 7, 2009; Revised Manuscript Received: May 27, 2009

The excited-state mono- and diproton transfer has been investigated in the S_1 state of [2,2′-bipyridyl]-3,3′-diol using the quantum mechanical resolution-of-identity second-order approximate coupled-cluster (RI-CC2) and time-dependent density functional theory (TDDFT) methods. Static investigation of stationary points and scans of the $\pi\pi^*$ and $n\pi^*$ energy surfaces have been performed. These calculations show that the concerted diproton transfer in S_1 proceeds along a ridge thus making this process highly unlikely since it will stabilize toward the unsymmetrical monoproton transfer. A small energy barrier of about 0.11 eV (RI-CC2 result) between the mono- and diketo structures is obtained allowing rapid continuation of the proton transfer to the diketo form. On-the-fly dynamics simulations performed at the RI-CC2 level confirm this picture. The first proton transfer step is so fast (7 fs) that it probably cannot be resolved by experimental techniques. Important participation of the $n\pi^*$ state is predicted. The present results shed a completely new light on the interpretation of the experimental results. The simulations clearly show that what has been experimentally determined as concerted transfer is in fact a combination of two sequential proton transfers separated by a small delay below the present experimental resolution. Concerning the second step of the sequential proton transfer the dynamics calculations indicate the existence of a highly dynamic system. Both the forward and reverse reactions of a monoketo/diketo equilibrium were found within the 300 fs period of the simulation. Environmental effects will certainly lead to a substantial cooling of the initially hot molecule and a concomitant decrease in the monoketo/diketo conversion rates, which will result in the experimentally observed overall time scale of 10 ps for the second proton transfer step.

1. Introduction

The excited-state intramolecular proton transfer (ESIPT) plays an important role for many chemical and biological processes.[1,2] A characteristic property of ESIPT is a large Stokes shift which leads to interesting applications for laser dyes and photostabilizers.[3−7] This Stokes shift signals strong structural changes in the excited state. Ultrafast (femtosecond) pump−probe experiments[1,8−12] together with extended theoretical investigations[7,12−17] have led to detailed insight into the mechanisms and time scales of ESIPT processes. The ESIPT mechanism normally includes the transfer of a hydroxyl (or amino) proton to an oxygen or nitrogen acceptor atom within a hydrogen bond already formed in the electronic ground state. Shifts in electron density after electronic excitation lead to significant enhancement in the acidity of the proton-donating group and in the basicity of the acceptor group thus facilitating the intramolecular proton transfer. In many cases this transfer is characterized by the absence of any energy barrier showing basically a vibrational relaxation mechanism in the excited state where the proton transfer proceeds as a ballistic wave packet motion on a time scale of less than 50 fs and involves skeletal deformations that modulate the donor−acceptor distance.[9,10,12,18] From the multitude of examples, 2-(2′-hydroxyphenyl)benzothiazole (HBT),[19] 10-hydroxybenzo[h]quinoline (HBQ),[12] and 2-(2′-hydroxyphenyl)benzotriazole (TIN-H)[7] relevant for the present investigations should be mentioned here.

SCHEME 1: Dienol (DE), Monoketo (MK) and Diketo (DK) Tautomers of [2,2′-Bipyridyl]-3,3′-diol ($BP(OH)_2$): (a) Current Scheme of $BP(OH)_2$ Dynamics Branched in Concerted and Sequential Reactions; (b) New Scheme Based on the Present Dynamics Simulations

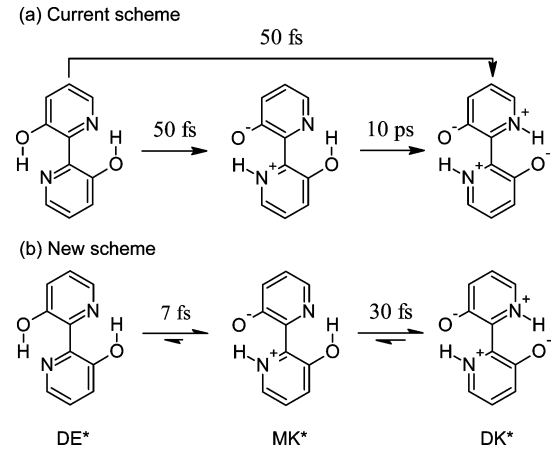

In these examples and in many others only a single proton transfer site exists. The compound [2,2′-bipyridyl]-3,3′-diol ($BP(OH)_2$) (Scheme 1) is of special interest since it contains two protons which can undergo proton transfer. It has been

* To whom correspondence should be addressed, hans.lischka@univie.ac.at.
† University of Vienna.
‡ Academy of Sciences of the Czech Republic.

10.1021/jp9032172 CCC: $40.75
Published on Web 07/02/2009

subject to several experimental[11,20−33] and theoretical[14,34−37] studies. Possible applications include usage as a laser dye[21] and as a probe in biological systems.[31,32] Derivatives of $BP(OH)_2$ could be effective polymer photostabilizers and solar energy collectors as well.[38] In the ground state the dienol (DE) structure is most stable. After photoexcitation two structures with emission wavelengths of 510 and 568 nm, which have been assigned to the diketo (DK) and monoketo (MK) forms, respectively, are present. The 568 nm structure disappears within 10 ps.[25] This fact is interpreted by the occurrence of a branched ultrafast reaction leading either to the monoketo (MK) or directly to the diketo (DK) structure followed by the conversion of MK to DK at a 10 ps time scale (see Scheme 1a).[25,30] Participation of a triplet state was excluded.[22] Two observations were presented for the existence of an additional relaxation channel. The MK to DK yield did not conform to the statistical limit of 2:1 for certain excitation energies[28] and a discrepancy between stimulated emission and transient absorption lifetimes was interpreted as participation of a $n\pi^*$ state with a nonradiative decay channel occurring at a time scale of 20 ps.[29] Recent pump−probe experiments using 30 fs time resolution performed by Stock et al.[11] shed more light on the initial ultrafast steps: analysis of the experiments were interpreted such that both the proton transfer from DE to MK and the direct DK process occurred at a similar time scale of about 50 fs. The fast time scale of the proton transfer was also taken as an indication of a barrierless process and a motion of a well-defined wavepacket on the excited state energy surface. However, it should be noted that previous femtosecond fluorescence upconversion experiments[28] were interpreted in terms of a DE to MK barrier of 300 cm^{-1}. It should also be mentioned that in the work of Stock et al.[11] no participation of a $n\pi^*$ state was found as opposed to the above-mentioned work of Neuwahl et al.[29] The measurements by Stock et al.[11] show coherent excitation of two symmetric and one antisymmetric in-plane skeletal modes. The antisymmetric mode is not directly affected by the Franck−Condon excitation but is taken as a direct sign for the symmetry breaking reaction of the monoproton transfer. The motion along totally symmetric normal modes was taken as evidence for the concerted diketo formation.

Several theoretical calculations have been published on the proton transfer in $BP(OH)_2$. The ground-state reaction has been studied by Barone and Adamo[34] by means of Hartree−Fock (HF) calculations. Sobolewski and Adamowicz[14] computed the ground-state potential energy surface (PES) and vertical excitation energies for the DE and DK forms. Calculations were performed at the HF, configuration interaction with single excitations (CIS), Møller−Plesset perturbation theory to second order (MP2), and complete active space perturbation theory to second order (CASPT2) levels. A barrierless diproton transfer reaction was predicted in the excited state, and the proximity of the $n\pi^*$ and $\pi\pi^*$ states was emphasized. Barone et al.[35] performed single point time-dependent density functional theory (TDDFT) on the DE and DK forms of $BP(OH)_2$ noting good agreement with experiment. Gelabert et al.[36] performed an excited state two-dimensional quantum dynamical study on a PES based on ground-state structures using the TDDFT/B3LYP method. Both a concerted and a sequential proton transfer are observed in the calculations. Whereas the time scale of about 20 fs for the concerted mechanism and the first step of the sequential one are found in good agreement with experiment, the computed time for the second proton transfer step in the sequential mechanism is considered to be significantly too fast due to the restriction to two degrees of freedom. When introducing an additional model coordinate, the authors of ref[36] noticed major changes in their results depending on the parameters used, an ambiguity which could not be resolved in their work. This problem can be overcome naturally through the present on-the-fly approach where all internal degrees of freedom are taken into account. Later on, the same group (Ortiz-Sánchez et al.[37]) used TDDFT/B3LYP for optimizing stationary points on the S_1 surface, an investigation which did not change, however, their just-described overall picture of the excited-state proton transfer mechanism in $BP(OH)_2$.

In previous systematic comparisons between TDDFT and resolution-of-identity second-order approximate coupled-cluster (RI-CC2)[39−41] results performed for a series of mono-ESIPT systems, it has been shown[13] that both methods are well suited for the description of this process. The significantly more time-consuming RI-CC2 calculations have been performed in this reference mostly as benchmark with the aim of assessing the validity of the TDDFT results. Several other investigations[42−44] also confirm the reliability of the RI-CC2 method for the calculation of excited states. On the basis of this experience, the TDDFT method had been used in investigations on the ESIPT process in HBT and HBQ[12,45] where static calculations on excitation and fluorescence energies and reaction paths had been combined with on-the-fly dynamics simulations. The resulting proton transfer times of 30−40 fs were found in excellent agreement with femtosecond pump−probe experiments.[9,12] Furthermore, the occurrence of ultrafast radiationless deactivation processes in HBT as observed in the gas phase[45] were explained by torsional interring motion leading to a conical intersection (see also related investigations for TIN-H in refs 7 and 46).

In this work we use the same just-described approaches which have already been applied successfully to monoproton transfer processes for investigations on the mono- and diproton transfer processes in $BP(OH)_2$. It was our objective to reinvestigate its potential energy surface in the first excited singlet state with respect to the ESIPT at the RI-CC2 level in order to assess the performance of the TDDFT method also in the present case. On-the-fly excited-state dynamics simulations were performed not only with the TDDFT method but also with the more advanced RI-CC2 approach. Whereas TDDFT has been applied previously for investigations on $BP(OH)_2$,[35−37] the RI-CC2 method used here offers an increased level of sophistication for the description of the dynamics of this system. The investigations give a direct picture of the proton transfer mechanisms especially concerning the competition of concerted diketo formation versus a sequential mechanism.

2. Computational Details

The TDDFT/B3LYP[47−50] and RI-CC2[39−41] calculations were carried out with the Turbomole 5.9 program package.[51] Two basis sets were used: the triple-ζ valence polarization (TZVP)[52] basis and a combination of the split valence polarized (SVP) basis[53] for heavy atoms and hydrogens involved in the ESIPT and a split valence (SV) basis[53] for the remaining hydrogen atoms (SVP-SV). Adiabatic molecular dynamics simulations and spectra generation have been performed with the Newton-X program package.[54,55] Solvent effects on excitation energies were computed for cyclohexane using the polarizable continuum method (PCM)[56,57] as implemented in the Gaussian package.[58] For this purpose single-point PCM/TDDFT/B3LYP/SVP computations, equilibrated for the excited state, were performed for the fully relaxed RI-CC2/TZVP structures in the $S_1(\pi\pi^*)$ state. Thermodynamic data such as ΔH_{gas} and ΔG_{gas} were computed

TABLE 1: Vertical Excitation and Fluorescence Energies (eV) Computed at Different Levels of Theory[a]

		TDDFT/B3LYP			RI-CC2		
geometry	state[b]	SVP-SV	TZVP	state[b]	SVP-SV	TZVP	exptl[c]
g.s.	$1\ ^1B_u$	3.737 (3.38×10^{-1})	3.767 (3.49×10^{-1})	$1\ ^1B_u$	3.901 (3.75×10^{-1})	3.880 (3.69×10^{-1})	3.647
g.s.	$1\ ^1A_u$	4.305 (1.45×10^{-3})	4.362 (2.62×10^{-3})	$2\ ^1A_g$	4.685 (0)	4.626 (0)	
g.s.	$2\ ^1A_g$	4.559 (0)	4.552 (0)	$1\ ^1A_u$	4.686 (1.51×10^{-3})	4.704 (1.77×10^{-3})	
g.s.	$3\ ^1A_g$	4.668 (0)	4.658 (0)	$3\ ^1A_g$	5.402 (0)	5.304 (0)	
g.s.	$2\ ^1B_u$	5.057 (5.83×10^{-2})	5.041 (5.96×10^{-2})	$1\ ^1B_g$	5.506 (0)	5.466 (0)	
g.s.	$1\ ^1B_g$	5.143 (0)	5.124 (0)	$2\ ^1B_u$	5.618 (9.44×10^{-2})	5.530 (9.89×10^{-2})	
g.s.	$2\ ^1B_g$	5.462 (0)	5.443 (0)	$2\ ^1B_g$	5.960 (0)	5.900 (0)	
MK	$1\ ^1A'$	2.466 (1.48×10^{-1})	2.409 (1.47×10^{-1})	$1\ ^1A'$	2.488 (3.11×10^{-1})	2.429 (2.96×10^{-1})	2.183
DK	$1\ ^1B_u$	2.708 (3.40×10^{-1})	2.690 (3.63×10^{-1})	$1\ ^1B_u$	2.599 (3.98×10^{-1})	2.547 (3.88×10^{-1})	2.431

[a] Oscillator strengths are shown in parentheses. [b] $\pi\pi^*$ states have A_g or B_u symmetry, $n\pi^*$ states A_u or B_g symmetry in the C_{2h} structures. [c] Reference 25.

within the standard harmonic oscillator/rigid rotator/ideal gas approximation. ΔG_{solv} values in solution were obtained by adding to ΔG_{gas} the solvent correction from the PCM calculation in the S_1 state.

Stationary points were optimized at the TDDFT/SVP-SV, TDDFT/TZVP, RI-CC2/SVP-SV, and RI-CC2/TZVP levels. In the first three cases all stationary points were characterized by harmonic analysis. In the last case the harmonic analysis was performed for the fully relaxed MK and DK structures and the planar DK minimum of the $S_1(\pi\pi^*)$ state. Unless specified differently, geometry optimizations were performed using C_s symmetry restriction.

Absorption and spontaneous emission spectra were calculated using a sample of geometries created by a Wigner distribution of a quantum harmonic oscillator as described in ref 55 using about 1000 geometries in each case. The spectral simulations were performed for the DE structure in its ground state for absorption and for the MK and DK structures, respectively, in their S_1 excited states for emission.

A two-dimensional scan of the potential energy surface was computed at the RI-CC2/SVP-SV level for the $S_1(\pi\pi^*)$ state in terms of the two OH distances. The two OH distances were fixed at each point and the remaining geometry was optimized under planarity restriction. The grid was constructed for OH distances between 1.7 and 3.7 au (step width, 0.2 au) consisting of 66 unique points. For the same geometries the energy of the $S_2(n\pi^*)$ state was computed as well. The energy was plotted against the reaction coordinates ΔR_i defined as

$$\Delta R_i = R_{OH,i} - R_{NH,i} \qquad (i = 1, 2) \tag{1}$$

where $R_{NH,i}$ and $R_{OH,i}$ are the two NH and OH distances, respectively (Scheme 1).

The on-the-fly dynamics simulations including all molecular degrees of freedom were performed using the TDDFT/B3LYP/SVP-SV and RI-CC2/SVP-SV methods, respectively, for the energy and energy gradient calculations. Initial conditions for the nuclear positions and momenta were generated according to a Wigner distribution of the harmonic vibrational ground state as described for the spectra calculations and transferred to the first electronically excited singlet state where the adiabatic dynamics was performed. One hundred trajectories were computed at the TDDFT level. Due to the significantly enhanced computer time of the RI-CC2 method as compared to TDDFT, 36 trajectories were calculated at the former level. A simulation time of 100 fs with a 0.5 fs time step was used in both cases. Additionally, 11 RI-CC2 trajectories were extended up to 300 fs.

In order to analyze the symmetry breaking due to the monoproton transfer in the dynamics simulation, each of the two proton transfer sites of $BP(OH)_2$ was labeled as active or inactive. The active site is the one where the first proton transfer occurs which is characterized by equal OH and NH distances ($\Delta R_i = 0$). According to this threshold the different species classified in the analysis of trajectories were defined as follows: (i) DE with both $\Delta R_i < 0$, (ii) MK with one $\Delta R_i > 0$ and the other $\Delta R_i < 0$, and (iii) DK with both $\Delta R_i > 0$.

The trajectories were characterized by a normal-mode analysis (NMA) similar to the one described by Kurtz et al.[59] First, the atoms in $BP(OH)_2$ were renumbered such as to have the proton transfer in the same OH···N bond. Then, at each time step the structures were aligned with the DK minimum using a least-squares fit based on quaternions[60] to remove translation and rotation. For each trajectory i and time step t the Cartesian difference vector $\mathbf{x}(i,t)$ between that structure and the DK reference geometry ($\mathbf{x}_0$) was converted to $\mathbf{y}(i,t)$ in the normal mode basis by the relation

$$\mathbf{y}(i,t) = \mathbf{V}^{-1}(\mathbf{x}(i,t) - \mathbf{x}_0) \tag{2}$$

where $\mathbf{V}^{-1}$ is the transformation matrix from Cartesian to normal coordinates.

For out-of-plane modes the absolute value of the displacement was taken since for a planar molecule the out-of-plane motion into both directions is equivalent. To characterize the $\mathbf{y}(i,t)$ vectors, they were first averaged over all trajectories and second the standard deviation over time of this time-dependent average was computed.

3. Results and Discussion

3.1. Vertical Excitations and Optimized Structures. Vertical excitation energies of the first seven excited states are collected in Table 1. The most intense transition is to the S_1 ($\pi\pi^*$) state and can be characterized as a highest occupied molecular orbital−lowest unoccupied molecular orbital (HOMO−LUMO) excitation. The excitation energy computed with different methods agrees quite well with the experimental absorption maximum of 3.647 eV.[25] Several states of $\pi\pi^*$ and $n\pi^*$ character follow S_1 and possess zero or small oscillator strength. The next state with larger oscillator strength is the $2\ ^1B_u$ state which is S_5 at TDDFT and S_6 at RI-CC2 level, respectively. This corresponds probably to the second peak in the absorption spectrum that is found below 267 nm.[28] It is noted that the RI-CC2 excitation energies are generally somewhat higher than the TDDFT results. Basis set dependence is not very pronounced.

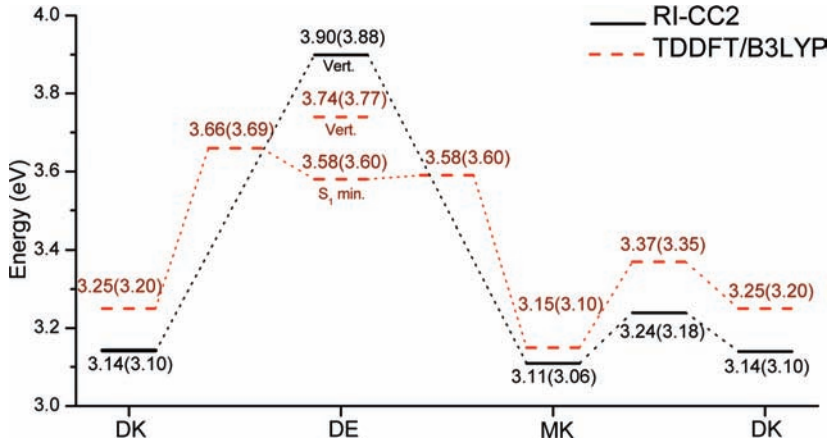

Figure 1. S_1 ($\pi\pi^*$) energies of the stationary points computed at the TDDFT/B3LYP and RI-CC2 levels using the SVP-SV and TZVP basis sets. TZVP results are shown in parentheses.

The TDDFT/B3LYP/TZVP results are in good agreement with a similar study of Ortiz-Sanchez et al.[37] The vertical excitation is 3.77 eV (TZVP result) and a shallow planar DE minimum is found below the Franck−Condon point at 3.60 eV (see also the energy scheme shown in Figure 1). The planar MK form is 0.10 eV lower than the DK structure. If torsion is allowed, MK relaxes in the $\pi\pi^*$ state through interring torsion to a structure of almost degenerate S_1 and S_0 energies where the TDDFT/B3LYP/TZVP method finally fails. With the SVP-SV basis set there is a shallow MK minimum 0.06 eV below the planar structure at an NCCN torsion angle of 146°.

At the RI-CC2/TZVP level the vertical excitation energy is close to 3.9 eV. The Franck−Condon structure relaxes directly to the MK or DK structures, which are about equal in energy (see Figure 1). No DE energy minimum is found in the excited state. Between the MK and DK minima there is a small barrier of 0.11 eV. In comparison, the TDDFT/B3LYP/TZVP barrier height is significantly higher with a value of 0.22 eV. The vibrational analysis performed at the RI-CC2/SVP-SV level shows that the planar DK structure is a minimum whereas the planar MK structure has two imaginary frequencies for pyramidalization ($183i$ cm^{-1}) and torsion ($33i$ cm^{-1}). The fully optimized $\pi\pi^*$ MK structure displays a small pyramidalization of the bridge carbon on the N-protonated ring and a slight interring torsion. The energetic effects of these distortions are very small. The RI-CC2/SVP-SV MK-DK transition state is not planar either as can be seen by the fact that its structure is a second-order saddle point which, aside from the transition mode ($1103i$ cm^{-1}), shows an imaginary pyramidalization ($129i$ cm^{-1}) mode also similar to the one in the MK form. At the RI-CC2/TZVP level neither the MK nor DK true energy minima are planar.

Thermodynamic data and solvent effects were computed for the MK/DK equilibrium at 298 K in the $S_1(\pi\pi^*)$ state in order to evaluate also its long-time behavior of the dynamics. For the fully relaxed MK and DK structures using the RI-CC2/TZVP approach the following results for the gas phase were obtained: $\Delta E_{gas} = 0.10$ eV, $\Delta H_{gas} = 0.086$ eV, and $\Delta G_{gas} = 0.095$ eV. Thus, at this computational level the MK form is slightly favored as opposed to the experimental results. Inclusion of the effect of cyclohexane, the solvent used in most experimental studies,[11,25,28] leads to a reversal of the equilibrium with a $\Delta G_{solv} = -0.049$ eV. It should be noted at this point that the energetic effects are very subtle and at the limit of the accuracy of the quantum chemical methods available for the size of molecules such as $BP(OH)_2$. Thus, deducing information about the molecule in thermal equilibrium is highly challenging because an accuracy in the order of the energy available at room temperature ($RT = 0.025$ eV) is required as opposed to the initial processes where a much larger vibrational excess energy of about 0.7 eV is available. Fortunately, the long-scale dynamics is already very well understood and in particular the quantitative formation of DK as the fluorescent species is firmly established.[20,23,25]

Selected optimized geometry data of the energy minima are shown in Figure 2. Full Cartesian RI-CC2 and TDDFT geometries for all stationary points are reported in the Supporting Information. Except for the DE ground state, all other structures are computed for the S_1 state which had either $\pi\pi^*$ or $n\pi^*$ character as specified. The structures for the $n\pi^*$ state will be discussed in the next paragraph. In the following, the RI-CC2/TZVP and TDDFT/B3LYP/TZVP results will be discussed with the TDDFT values shown in parentheses. In the DK tautomer the inter-ring CC bond is shortened by 0.07 Å (0.06 Å) as compared to the ground state. This shortening is consistent with the fact that the LUMO orbital shows a bonding contribution for the inter-ring CC bond (cf. ref 35). Formation of the keto structure is seen from a shortening of the CO distance by 0.04 Å (0.07 Å). This behavior was also observed for HBT.[45] In the MK tautomer the inter-ring CC distance decreases by 0.02 Å with RI-CC2 and increases by 0.04 Å with TDDFT as compared to the ground-state geometry. In the MK structure the HOMO and LUMO are localized on different rings. The formation of the keto structure reduces the CO bond by 0.02 Å (0.07 Å). The intact OH···N hydrogen bond length increases by 0.05 Å (0.09 Å). To allow a closer comparison between methods, hydrogen bond lengths of structures computed with planarity restriction are summarized in Table 2 for different levels of theory. Bond distances computed with the RI-CC2 method are significantly smaller than those obtained at the (TD)DFT level. This effect amounts to about 0.02−0.04 Å in the electronic ground state and increases to above 0.1 Å for the N···H bond length in the MK structure in the S_1 state. A similar trend was also found in a previous study on a series of ESIPT cases.[13] The hydrogen bond lengths increase when a larger basis set is used which is probably related to a decrease in the basis set superposition error. Similar experience has already been made before.[61] The absence of an excited state DE minimum at the RI-CC2 level could be explained by the presence of stronger hydrogen bonds which favors the proton transfer.

Even though the bright $\pi\pi^*$ state is decisive as concerns the initial acceleration of the wave packet and the first proton transfer, the dynamics simulations described below show that

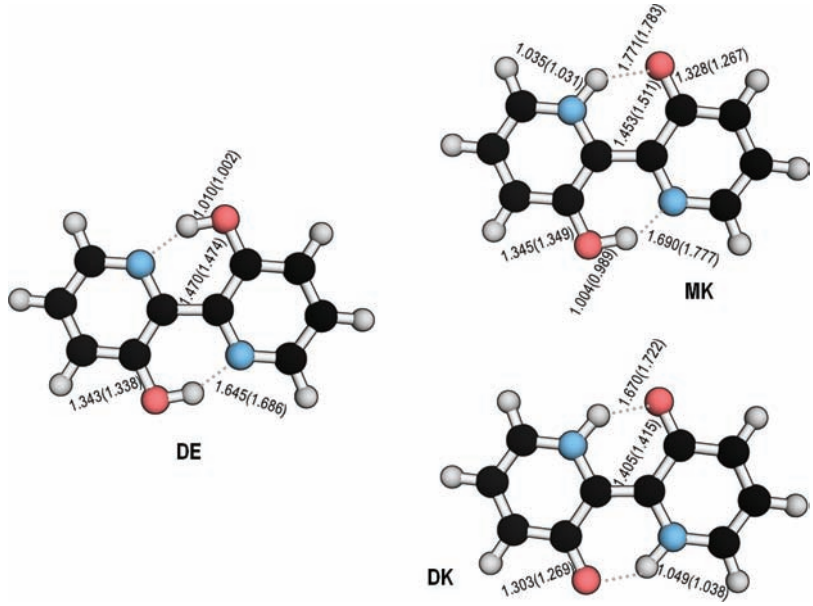

Figure 2. Ground-state (DE) and excited-state (MK, DK) optimized geometries computed at the RI-CC2/TZVP and (TD)DFT/B3LYP/TZVP levels, latter values in parentheses. DE and DK are planar (TDDFT and RI-CC2) whereas MK (RI-CC2/TZVP) shows an NCCN inter-ring torsion angle of 162°. The B3LYP/TZVP MK structure is restricted to planarity.

TABLE 2: Hydrogen Bond Lengths (Å) Computed with Different Methods for the DE (Ground State), MK, and DK (S_1 $\pi\pi^*$ state) Structures[a]

method	DE (N···H)	MK (O···H/N···H)	DK (O···H)
B3LYP/SVP-SV	1.658	1.751/1.741	1.696
B3LYP/TZVP	1.686	1.783/1.777	1.722
RI-CC2/SVP-SV	1.638	1.744/1.615	1.667
RI-CC2/TZVP	1.645	1.755/1.621	1.670

[a] Optimizations were performed with C_s restriction.

the nπ^* state plays an important role in the further progression of the dynamics. Therefore, in this paragraph, a discussion of relevant structures in the nπ^* state is presented. At the Franck−Condon geometry the nπ^* state, with the nonbonding orbital located on the nitrogen atoms, is about 0.6 eV higher in energy than the $S_1(\pi\pi^*)$ state. After transfer of one or two protons, the nπ^* state becomes competitive with the $\pi\pi^*$ state. Planar and true nonplanar S_1 minima of nπ^* character were found at the RI-CC2 level. At the planarity restricted RI-CC2/TZVP level, the energies of the S_1 nπ^* minima are 3.02 eV (DK) and 3.03 eV (MK) being slightly below the energies of the $\pi\pi^*$ structures (cf. Figure 1). Allowing nonplanar geometry relaxation leads to energies and NCCN torsional angles of 2.93 eV/167° (DK) and 2.89 eV/163° (MK). At the B3LYP/TZVP level with planarity restriction a true DK S_2 nπ^* (3.42 eV) and an MK minimum (3.23 eV) with one imaginary out-of-plane mode have been located. In this case energies are slightly higher than the corresponding $\pi\pi^*$ minima. With all the methods used the DK structure is bent and C_2 symmetry is lost. The electronic excitation comes from the n-orbital on the side of the longer hydrogen bond. In the MK structure lengthening of the O···H hydrogen bond with respect to the $\pi\pi^*$ minimum is observed which can be ascribed to the fact that an electron is taken out of an n-orbital of the oxygen atom forming that hydrogen bond. A summary of energies and structural parameters of $\pi\pi^*$ and nπ^* optimized geometries is given in the Supporting Information.

The inter-ring torsional potentials for the MK form of $BP(OH)_2$ are displayed in Figure 3 for the TDDFT/B3LYP/SVP and RI-CC2/SVP-SV methods. For each fixed NCCN torsional angle the remaining geometry has been optimized in the S_1 state. The S_1 state TDDFT curve shows a very flat reaction path apparently leading to a conical intersection. For the RI-CC2 curve the above-mentioned nonplanar energy minimum can be found at a torsional angle of about 175°. The curve is also very flat in this region. Beyond this point the S_1 curve increases steadily and a lowering of the S_1-S_0 gap is observed. Both curves show that activation of the inter-ring torsion will be unlikely and that ultrafast dynamics is not to be expected.

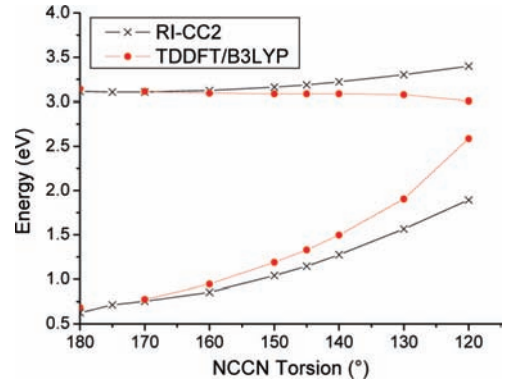

Figure 3. Torsional curves computed for fixed NCCN angle and optimized remaining geometry computed at the RI-CC2/SVP-SV and TDDFT/B3LYP/SVP levels.

Vertical fluorescence energies and lifetimes for spontaneous emission are presented in the last two rows of Table 1. The same ordering in fluorescence energies of the MK and DK forms as for the experimental values is found with a slight overall shift to higher values. To allow further comparison with experimental results, the vibrational structures of the spectra were simulated at the RI-CC2/SVP-SV level. Absorption bands computed for DE and emission spectra for MK and DK are depicted in Figure 4. The vertical excitation and emission energies show a non-negligible blue shift (DE, 0.06 eV; MK, 0.15 eV; DK, 0.05 eV) with respect to the computed band maxima. Comparison with the experimental band shapes given in ref 25 shows that our computational methods are able to reproduce them quite well. The results support the assignment

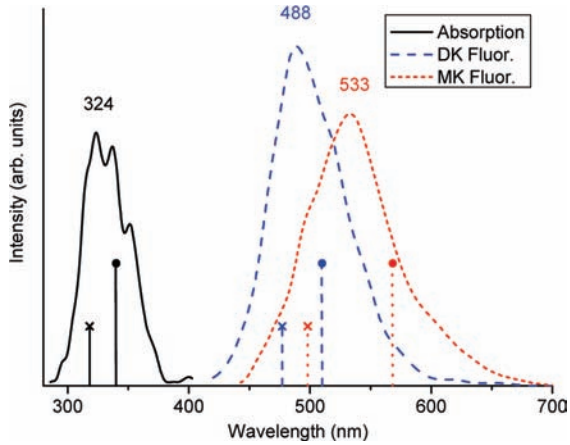

Figure 4. Simulated absorption and fluorescence spectra (RI-CC2/SVP-SV). Experimental band maxima[25] are indicated by circles, computed vertical excitation energies by crosses.

of the experimental bands of 510 and 568 to the DK and MK structures, respectively.[25]

3.2. Two-Dimensional Energy Grid for S_1 and S_2. A full two-dimensional grid of the potential energy surface (PES) in the coordinates ΔR_i (eq 1) was constructed at the RI-CC2/SVP-SV level (Figure 5) as described in the Computational Details. For the $\pi\pi^*$ state, Figure 5a shows a barrierless decline from the Franck−Condon region ($\Delta R_1 = \Delta R_2 = -0.626$ Å) to the MK and DK structures. The symmetric double transfer proceeds via an elongated shallow area for which the TDDFT method resulted in a local minimum. This symmetric path forms a ridge extending from the DE to the DK structure, which is instable toward an unsymmetric single proton transfer path forming the MK structure. Thus, only highly symmetric initial conditions could lead directly to the DK structure. That this is an exceptional case is shown in the dynamics calculations discussed in the next section. In the analogous TDDFT surface (not shown) there was even a second-order saddle point along the direct DE−DK path because of the DE minimum on the S_1 surface. This fact makes a symmetric transfer even more unlikely. The energy surface for the nπ^* state computed at the $\pi\pi^*$ geometries is shown in Figure 5b. This state is characterized by removing an electron from a nonbonding oxygen molecular orbital (MO). The general shape of this energy surface is very similar to the one computed for the $\pi\pi^*$ state, and the dynamics is expected to proceed in a similar way. The energy difference between these two excited singlet states is shown in Figure 5c. In the DE region a considerable energy gap of about 0.8 eV if observed. Close to the MK−DK transition state this gap reduces to only about 0.1 eV. Proximity between the first two singlet excited states was also found in our previous ESIPT studies[13] and has also been noted by Sobolewski and Adamowicz.[14]

In Table 3 selected harmonic frequencies for the ground state and the MK and DK structures in the S_1 state are collected and compared with the results obtained from the pump−probe experiments reported by Stock et al.[11] (See this work also for a characterization of these modes.) In their investigations these authors have used the DE ground-state frequencies for comparison with the experimental frequencies. Our calculations show that these ground-state DE frequencies actually have close counterparts in the MK and DK modes of the excited state.

3.3. Dynamics Simulations. At this point it should be recalled that the S_1 energy surface computed at the TDDFT/B3LYP and RI-CC2 levels shows in many regions a similar shape. Especially the ridge characterizing the symmetric double proton transfer was found with both methods. Major differences

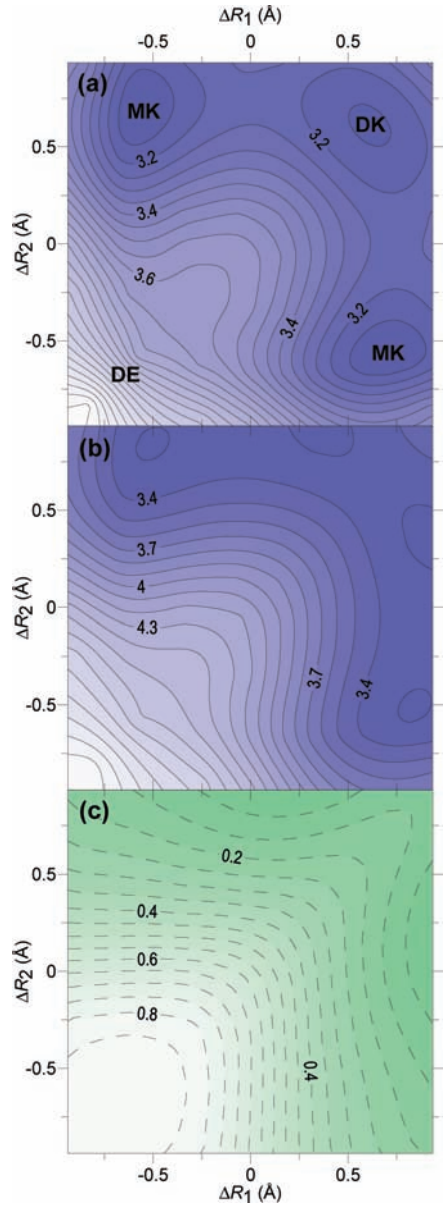

Figure 5. PES for (a) the $\pi\pi^*$ state and (b) the nπ^* state computed at the RI-CC2/SVP-SV level. Energies are given in electronvolts relative to the ground-state energy minimum. The difference between the two states is shown in (c).

TABLE 3: Wavenumbers (cm^{-1}) of Low-Frequency Normal Modes Computed at the RI-CC2/SVP-SV Level in Comparison with Analogous Experimental Frequencies Derived from Pump−Probe Experiments

DE (S_0)	213 ($20b_u$)	328 ($21a_g$)	360 ($20a_g$)
MK (S_1)	201, 215 (57a, 56a)[a]	318 (53a)	337 (52a)
DK (S_1)	169 ($20b_u$)	326 ($21a_g$)	352 ($20a_g$)
exptl(S_1)[b]	193 ($20b_u$)	294 ($21a_g$)	331 ($20a_g$)

[a] In the nonplanar MK two modes similar to the $20b_u$ were found. [b] Reference 11.

were the absence of a DE minimum in the S_1 state at the RI-CC2 level as opposed to the TDDFT approach. However, the TDDFT DE minimum was still recognizable by a corresponding shallow region in the RI-CC2 potential energy surface. The most remarkable differences (see Figure 1) between the results obtained with the two methods are found in the fact that with TDDFT the MK structure is significantly more stable than the DK structure, that a higher TDDFT MK to DK barrier (TDDFT/

SVP-SV, 0.21 eV vs RI-CC2/SVP-SV, 0.13 eV) exists, and that the kinetic energy available after electronic excitation for surmounting the MK−DK barrier (vertical excitation energy minus energy of the MK-DK saddle point) is much smaller for TDDFT (0.36 eV) in comparison to RICC2 (0.66 eV). The stronger torsion of the MK structure at the TDDFT level should also be kept in mind.

After the proton transfer in $BP(OH)_2$ was investigated in terms of relevant parts of the energy surface in the S_1 state, the results of the dynamics simulations are presented now. In this work classical on-the-fly dynamics were performed where all internal degrees of freedom are included. The importance of this multidimensionality has been emphasized several times in literature[12,45,62] and in particular the influence of skeletal modes has been described for $BP(OH)_2$.[11,27] Tunneling effects are certainly not important here since in the first proton transfer step no barrier is observed at all and for overcoming a small barrier in the second step there is by far sufficient kinetic energy available. The absence of isotope effects on deuteration[27] confirms this view. A detailed comparison of classical dynamics calculations with two-dimensional wavepacket simulations has been performed for HBQ[12] where in the latter case the two degrees of freedom were used for the description of the single intramolecular hydrogen bond occurring in this system. Results show good overall agreement between the two approaches in the initial phase of the dynamics. However, the limitations of the two-dimensional wavepacket approach in terms of missing energy dissipation to other degrees of freedom have been noted in that work as well, very similar to those found in the wavepacket dynamics simulations on $BP(OH)_2$[36] discussed above.

In the following analysis an assignment of different geometries to the DE, MK, and DK structures (see Computational Details for definition) obtained during the dynamics was performed. Figure 6 displays the time evolution of these species. With the RI-CC2 method the DE population drops rapidly after an initial phase of 3 fs and MK is formed. After 18.5 fs, less than 10% of the DE is present. At about 30 fs the concentration of MK shows a maximum and starts transforming into DK. At 60 fs a small amount of the DE form reappears. This reappearance could be related to the observations of Toele et al.[30] who found in their fluorescence anisotropy study a 350 fs decay component when probing at 460 nm, which was assigned to the DE structure. Analysis of the simulations indicates that these DE molecules do not come from structures trapped in the Franck−Condon region but rather from a reflection back into the DE area. After 100 fs 63% of the RI-CC2 trajectories show a MK structure and 37% the DK form.

The situation is quite different in the TDDFT dynamics. The DE decay is considerably slower and the time for 90% conversion is 42.5 fs, more than twice of that for RI-CC2. DK is hardly formed constituting only 5% after 100 fs. The absence of DK formation can be attributed to the facts listed at the beginning of this section: the higher stability of MK vs DK, the higher barrier in TDDFT as compared to RI-CC2, and the smaller amount of kinetic energy available. This simulation outcome, which is contrary to the experiments[11,30] is an indicator that the TDDFT/B3LYP combination is not useful in this particular case.

In Figure 7 the average values of ΔR_i are plotted against time. A sharp increase in ΔR_i due to the monoproton transfer can be seen for the value on the active side. After only 7 fs the average value of the reaction coordinate for the active side is already zero, i.e., $R_{OH} = R_{NH}$. This condition has previously been taken as a measure for the proton transfer time.[12] On the other (inactive) side a gradual increase in ΔR_i is seen as in some of the trajectories the DK structure is already formed.

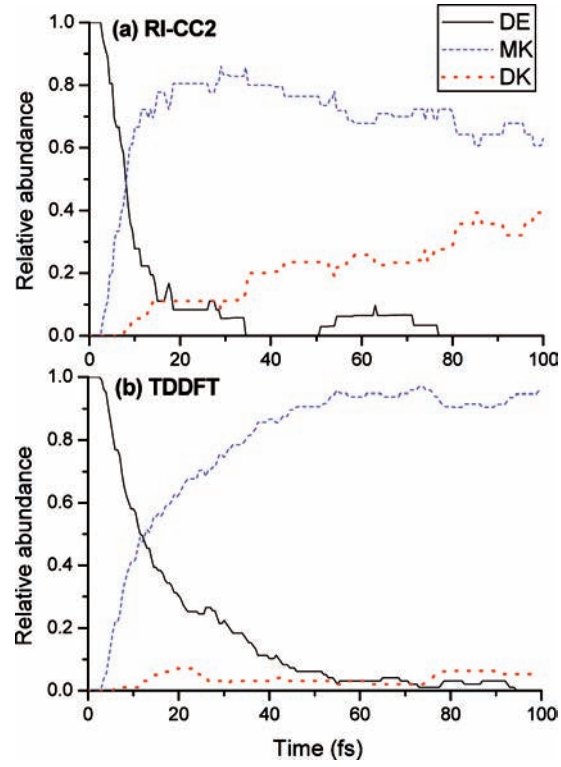

Figure 6. Time dependence of the relative abundances of the DE, MK, and DK species computed at the RI-CC2 (a) and TDDFT (b) levels.

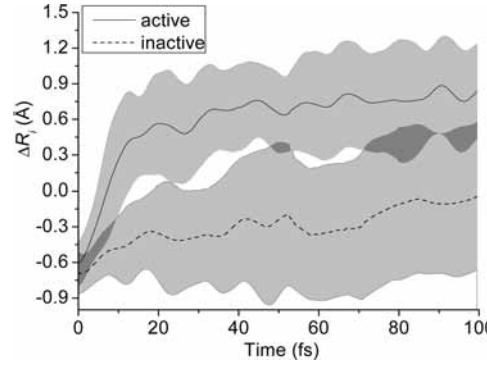

Figure 7. Time evolution of the proton transfer coordinate ΔR_i averaged over all trajectories. "Active" refers to the side of the first proton transfer. Grey areas indicate ± one standard deviation around the average.

To illustrate the question of sequential vs concerted transfer in more detail, the RI-CC2 trajectories have been projected into the $\Delta R_1/\Delta R_2$ plane (Figure 8). In this diagram the DE structure is found in the lower left corner, DK is located on the right top, and the two equivalent MK structures are situated in the two remaining corners. A symmetric concerted transfer corresponds to the DE−DK diagonal in this graph. Actually, only two trajectories are found in this region. Paths along the sides mark the first and second steps in asymmetric sequential transfers and constitute by far the majority of the trajectories. All the processes along the sides, i.e., single transfers including back reactions, take place readily. On average 2.0 proton transfers (as defined in the computational details) per trajectory were observed during the first 100 fs: 1.2 DE → MK, 0.5 MK → DK, 0.2 DK → MK, and 0.2 MK → DE.

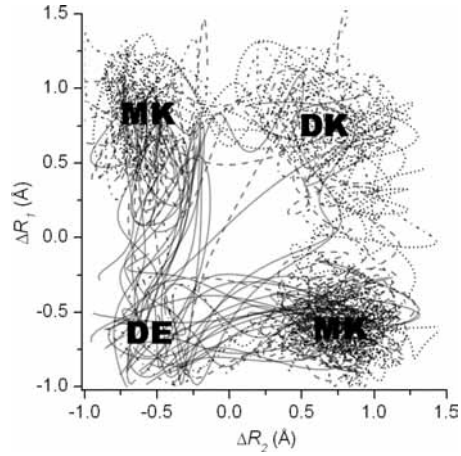

Figure 8. Projection of the trajectories onto the $\Delta R_1/\Delta R_2$ plane. Time coding: —, 0−25 fs; - - -, 25−50 fs; - . -, 50−75 fs; ..., 75−100 fs.

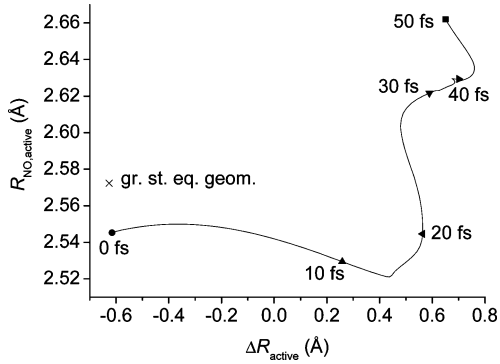

Figure 9. Time dependence of the average NO distance $R_{NO,active}$ plotted against the average value of the reaction coordinate ΔR_{active}.

It is well documented in the literature that the excited-state proton transfer may be supported by skeletal motions.[12,45,62] For molecules such as HBT and HBQ,[12] the rapid proton transfer takes place after slower skeletal motions generate a suitable geometry. The distance of the heavy atom of the proton donor group to the acceptor atom (the NO distance in this case) is used also here to describe these skeletal motions. In Figure 9 the initial part of the dynamics dealing with the first proton transfer step is analyzed. The average distance $R_{NO,active}$ is plotted against ΔR_{active} (eq 1). The index "active" indicates that the average has been performed always for the active side of the first proton transfer of the molecule.

It should be noted that the average initial value of $R_{NO,active}$ is 0.03 Å shorter than the ground-state equilibrium value. This shortening can be explained by the fact that from the random initial geometries the side with the shorter NO distance is favored in becoming the active side. The proton transfer will occur preferentially on the OH group with the initially smaller ON distance. Thus, the proton transfer in $BP(OH)_2$ will proceed much faster than in case of a mono-hydrogen-bonded compound since on the average always the OH group closer to the acceptor site will show the transfer. This situation thus represents a competitive advantage over the mono-hydrogen-bonded systems where such a possibility is absent. The short proton transfer time of about 7 fs as compared to 36 fs for HBT and 30 fs for HBQ confirms these conclusions.

The pump−probe experiments of Stock et al.[11] result in a significantly larger proton transfer time of about 50 fs for $BP(OH)_2$. We can identify two main reasons for this discrepancy. The first is assigned to the fact that in our simulations the condition $\Delta R_i = 0$ is tested while the experiment monitors changes in the induced emission, which is related to changes in the electronic structure and the potential energy of the new species. For species like HBT, for which the skeletal deformation occurs simultaneously to the ESIPT[12] these times agree well. Nevertheless, as we have seen, for $BP(OH)_2$ the ESIPT occurs in only 7 fs according to geometrical conditions without giving time for extensive further skeletal relaxation. This should create a delay between the ESIPT and the changes in the transmission signal. Second, the dynamics shows that the nπ* state is largely populated. The fraction of the population in the dark nπ* state will barely contribute to the stimulated emission, which should also have the effect of increasing the fitted time parameters. Uncertainties in the simulation results due to the quantum chemical methods employed but also in the experimental fittings should be kept in mind.

The most important coherent motions in the dynamics have been determined through normal-mode analysis. The standard deviation of averaged displacement vectors with respect to the DK reference geometry (see Computational Details) are shown in Figure 10. All of the out-of-plane modes (a_u, b_g) show only negligible coherent activity as there is no significant change in the corresponding force constants. Strong coherent activities are found only for in-plane modes with the most prominent ones being the $20b_u$, $21a_g$, and $20a_g$ modes. The same three modes have also been found in the analysis of the recent femtosecond pump−probe investigations.[11] They correspond to symmetric and antisymmetric in-plane skeletal motions leading to proton

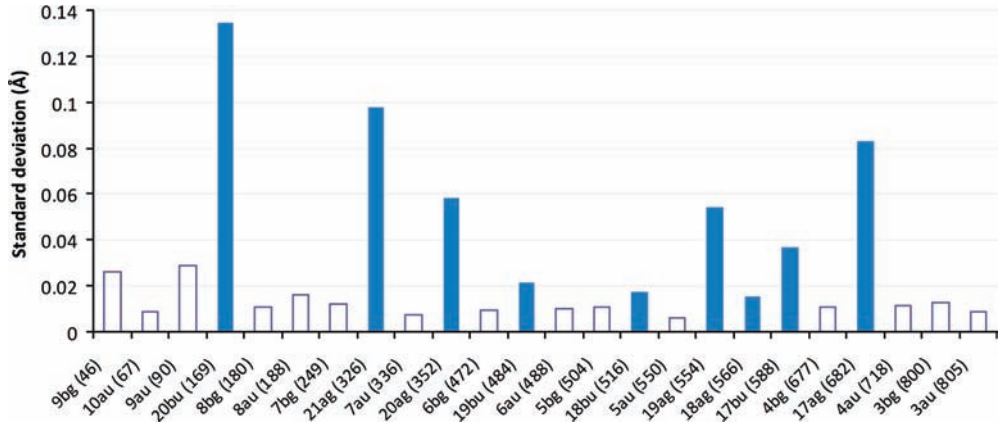

Figure 10. Coherent normal mode activity during the dynamics simulation as measured by the standard deviation of averaged displacement vectors with respect to the DK reference geometry. Vibrational frequencies are given in parentheses (cm^{-1}). In-plane modes are shown as solid bars, out-of-plane modes as empty bars.

transfer. According to the Franck−Condon rules a nontotally symmetric mode cannot be excited by an allowed transition. Its activity stems from the reactive process itself, and therefore, this is a strong indication for the symmetry breaking occurring in the proton transfer.[11] Furthermore it is noted that strong participation of the symmetric $21a_g$ mode is not necessarily in contradiction to the fact that the process itself does not conserve the C_{2h} symmetry.

Finally, the question of an additional relaxation channel will be addressed. During the simulation, switches between the $\pi\pi^*$ and $n\pi^*$ character of the S_1 state were observed. Between simulation times of 30−65 fs the distribution between these two states was about even. After 100 fs, 81% of the trajectories had switched to the $n\pi^*$ state. Moreover, 19% of the trajectories had S_1-S_0 energy gaps below 1 eV, all of them in the $n\pi^*$ state. The simulations indicate that the lowering of the gap occurs through H out-of-plane motion in the MK form. The simulations give support to the findings of Neuwahl et al.[29] that partial conversion to the dark $n\pi^*$ state and then on to the ground state may happen. The switching of the state character does not seem to imply other significant changes in the dynamics. In particular MK and DK structures and proton transfers are observed in both states. It is interesting to compare this to a recent study on *o*-hydroxybenzaldehyde[17] where it was observed that the switch into the $n\pi^*$ state significantly increased the barrier and essentially stopped the proton transfer. The difference in the present case is probably that excitation comes from an orbital on the far side of the proton transfer which should not have as much impact on the process.

4. Conclusions

Extended quantum chemical investigations on the excited-state proton transfer process in [2,2′-bipyridyl]-3,3′-diol ($BP(OH)_2$) have been performed using the RI-CC2 and TDDFT/B3LYP methods with the aim of establishing benchmark results for the energy surface in the first excited singlet state to be used for dynamics simulations performed in this work as well. Main attention is given to the question of the sequential versus concerted proton transfer. The results obtained by the two methods are in some aspects quite similar. Both RI-CC2 and TDDFT calculations show a clear preference for a sequential proton transfer mechanism since the concerted diproton transfer is unstable as it would proceed on a ridge of the energy surface in the coordinate space of the two proton transfer coordinates. Energetic stabilization will prefer the single proton transfer. No energy barrier on the dienol to monoketo pathway is observed in contrast to conclusions drawn from femtosecond fluorescence upconversion experiments.[28] The monoketo (MK) and diketo (DK) forms are local minima on the S_1 surface. The most extended calculations (RI-CC2/TZVP) show that they possess about equal stability. The two structures are separated by a barrier of 0.11 eV (RI-CC2/TZVP). The TDDFT results show an energetic preference for the MK structure by 0.14 eV and a MK to DK energy barrier of 0.25 eV. The available kinetic energy for the MK to DK transfer is about 0.3 eV larger at the RI-CC2 level.

As illustrated in Scheme 1b, dynamics results show practically exclusive DE to MK conversion on the S_1 energy surface with a slight reappearance of DE and the MK/DK equilibrium. The dynamics simulations performed at the TDDFT/B3LYP and RI-CC2 levels confirm that the first step in the proton transfer is always a single proton transfer leading to the monoketo structure. Only a very small fraction of direct symmetric double proton transfer was observed. The first proton transfer step is very fast occurring in the RI-CC2 simulations within about 7 fs as compared to previous proton transfer times for monohydrogen bonded systems such as HBT (36 fs) and HBQ (30 fs).[12] This difference can be explained by a competitive advantage of a dihydroxy over a monohydroxy compound, where the former can utilize more efficiently initial asymmetries in skeletal motions facilitating the proton transfer. In the first 300 fs—the maximum time of our simulations—the system can be described as a dynamic equilibrium between the monoketo and diketo structures since frequent exchanges between the two structures were observed. Therefore, for the second proton transfer step a straightforward definition of the transfer time cannot be given. The maximum of the MK population (see Figure 6) occurring at 30 fs has been chosen in Scheme 1. A normal-mode analysis of the average displacements along the trajectories shows that despite the entirely asymmetric proton transfer mechanism also symmetric modes are active and thus their participation is not in contradiction to this mechanism. The frequencies and character of the major normal modes determined are in good accord with the analysis of a recent 30 fs time resolution study.[11] Strong evidence for participation of the $n\pi^*$ state has been provided as well.

The present results, summarized in Scheme 1b, shed a completely new light on the interpretation of the experimental results. The simulations show that what has been experimentally assigned to a concerted transfer[11,25,30] is in fact a combination of two sequential proton transfers separated by a small delay below the present experimental resolution. The RI-CC2 simulations indicate the existence of a highly dynamic system rather than one consisting of two distinct reaction branches. Both, the forward and reverse reactions of a MK−DK equilibrium were found within the 300 fs period of the simulation. The DK → MK reverse reaction has so far been not yet included into the kinetic analysis of the experimental results. With the high effective initial temperature of about 4200−7700 K the barrier of about 0.1 eV can be easily overcome in both directions and, therefore, a MK/DK equilibrium should be feasible. It should be noted that the present dynamics simulations have been performed in gas phase and no energy dissipation into or polarization by the solvent was included. Environmental effects will certainly lead to a substantial cooling of the initially hot molecule and a concomitant decrease in the MK/DK conversion rates, which will result in the experimentally observed overall time scale of 10 ps for the second proton transfer step. Polarization by the solvent was shown to have only a minor effect compared to the initial excess energy and is in particular not expected to influence the first steps in the dynamics.

Acknowledgment. This work was supported by the Austrian Science Fund within the framework of the Special Research Program F16 (Advanced Light Sources) and Project P18411-N19. Support by the grant from the Ministry of Education of the Czech Republic (Center for Biomolecules and Complex Molecular Systems, LC512) and by the Praemium Academiae of the Academy of Sciences of the Czech Republic, awarded to Pavel Hobza in 2007, is gratefully acknowledged. This work was part of the research project Z40550506 of the Institute of Organic Chemistry and Biochemistry of the Academy of Sciences of the Czech Republic. The calculations were partially performed at the Linux PC cluster Schrödinger III of the computer center of the University of Vienna.

Supporting Information Available: Energetic and geometric information, total energies, and Cartesian geometries of structures optimized at the RI-CC2/TZVP and B3LYP/TZVP

levels. This material is available free of charge via the Internet at http://pubs.acs.org.

References and Notes

(1) Douhal, A.; Lahmani, F.; Zewail, A. H. *Chem. Phys.* **1996**, *207*, 477.

(2) Formosinho, S. J.; Arnaut, L. G. *J. Photochem. Photobiol., A* **1993**, *75*, 21.

(3) Barbara, P. F.; Brus, L. E.; Rentzepis, P. M. *J. Am. Chem. Soc.* **1980**, *102*, 5631.

(4) Laermer, F.; Elsaesser, T.; Kaiser, W. *Chem. Phys. Lett.* **1988**, *148*, 119.

(5) Arthenengeland, T.; Bultmann, T.; Ernsting, N. P.; Rodriguez, M. A.; Thiel, W. *Chem. Phys.* **1992**, *163*, 43.

(6) Douhal, A. *Acc. Chem. Res.* **2004**, *37*, 349.

(7) Sobolewski, A. L.; Domcke, W.; Hättig, C. *J. Phys. Chem. A* **2006**, *110*, 6301.

(8) Stock, K.; Bizjak, T.; Lochbrunner, S. *Chem. Phys. Lett.* **2002**, *354*, 409.

(9) Lochbrunner, S.; Wurzer, A. J.; Riedle, E. *J. Phys. Chem. A* **2003**, *107*, 10580.

(10) Takeuchi, S.; Tahara, T. *J. Phys. Chem. A* **2005**, *109*, 10199.

(11) Stock, K.; Schriever, C.; Lochbrunner, S.; Riedle, E. *Chem. Phys.* **2008**, *349*, 197.

(12) Schriever, C.; Barbatti, M.; Stock, K.; Aquino, A. J. A.; Tunega, D.; Lochbrunner, S.; Riedle, E.; de Vivie-Riedle, R.; Lischka, H. *Chem. Phys.* **2008**, *347*, 446.

(13) Aquino, A. J. A.; Lischka, H.; Hattig, C. *J. Phys. Chem. A* **2005**, *109*, 3201.

(14) Sobolewski, A. L.; Adamowicz, L. *Chem. Phys. Lett.* **1996**, *252*, 33.

(15) Coe, J. D.; Levine, B. G.; Martinez, T. J. *J. Phys. Chem. A* **2007**, *111*, 11302.

(16) Migani, A.; Bearpark, M. J.; Olivucci, M.; Robb, M. A. *J. Am. Chem. Soc.* **2007**, *129*, 3703.

(17) Coe, J. D.; Martinez, T. J. *Mol. Phys.* **2008**, *106*, 537.

(18) Lochbrunner, S.; Schriever, C.; Riedle, E. In *Hydrogen-Transfer Reactions*; Hynes, J. T., Klinman, J. P., Limbach, H.-H., Schowen, R. L., Eds.; Wiley-VCH: Weinheim, Germany, 2006; pp 349.

(19) de Vivie-Riedle, R.; De Waele, V.; Kurtz, L.; Riedle, E. *J. Phys. Chem. A* **2003**, *107*, 10591.

(20) Bulska, H. *Chem. Phys. Lett.* **1983**, *98*, 398.

(21) Sepiol, J.; Bulska, H.; Grabowska, A. *Chem. Phys. Lett.* **1987**, *140*, 607.

(22) Grabowska, A.; Borowicz, P.; Martire, D. O.; Braslavsky, S. E. *Chem. Phys. Lett.* **1991**, *185*, 206.

(23) Borowicz, P.; Grabowska, A.; Wortmann, R.; Liptay, W. *J. Lumin.* **1992**, *52*, 265.

(24) Wortmann, R.; Elich, K.; Lebus, S.; Liptay, W.; Borowicz, P.; Grabowska, A. *J. Phys. Chem.* **1992**, *96*, 9724.

(25) Zhang, H.; vanderMeulen, P.; Glasbeek, M. *Chem. Phys. Lett.* **1996**, *253*, 97.

(26) Glasbeek, M.; Marks, D.; Zhang, H. *J. Lumin.* **1997**, *72*−*4*, 832.

(27) Marks, D.; Zhang, H.; Glasbeek, M.; Borowicz, P.; Grabowska, A. *Chem. Phys. Lett.* **1997**, *275*, 370.

(28) Marks, D.; Prosposito, P.; Zhang, H.; Glasbeek, M. *Chem. Phys. Lett.* **1998**, *289*, 535.

(29) Neuwahl, F. V. R.; Foggi, P.; Brown, R. G. *Chem. Phys. Lett.* **2000**, *319*, 157.

(30) Toele, P.; Zhang, H.; Glasbeek, M. *J. Phys. Chem. A* **2002**, *106*, 3651.

(31) Abou-Zied, O. K. *J. Photochem. Photobiol., A* **2006**, *182*, 192.

(32) Abou-Zied, O. K.; Al-Hinai, A. T. *J. Phys. Chem. A* **2006**, *110*, 7835.

(33) Suresh, M.; Jose, D. A.; Das, A. *Org. Lett.* **2007**, *9*, 441.

(34) Barone, V.; Adamo, C. *Chem. Phys. Lett.* **1995**, *241*, 1.

(35) Barone, V.; Palma, A.; Sanna, N. *Chem. Phys. Lett.* **2003**, *381*, 451.

(36) Gelabert, R.; Moreno, M.; Lluch, J. M. *ChemPhysChem* **2004**, *5*, 1372.

(37) Ortiz-Sanchez, J. M.; Gelabert, R.; Moreno, M.; Lluch, J. M. *ChemPhysChem* **2007**, *8*, 1199.

(38) Kaczmarek, L.; Borowicz, P.; Grabowska, A. *J. Photochem. Photobiol., A* **2001**, *138*, 159.

(39) Christiansen, O.; Koch, H.; Jorgensen, P. *Chem. Phys. Lett.* **1995**, *243*, 409.

(40) Hättig, C. *J. Chem. Phys.* **2003**, *118*, 7751.

(41) Köhn, A.; Hättig, C. *J. Chem. Phys.* **2003**, *119*, 5021.

(42) Schreiber, M.; Silva, M. R.; Sauer, S. P. A.; Thiel, W. *J. Chem. Phys.* **2008**, 128.

(43) Fleig, T.; Knecht, S.; Hattig, C. *J. Phys. Chem. A* **2007**, *111*, 5482.

(44) Sobolewski, A. L.; Shemesh, D.; Domcke, W. *J. Phys. Chem. A* **2009**, *113*, 542.

(45) Barbatti, M.; Aquino, A. J. A.; Lischka, H.; Schriever, C.; Lochbrunner, S.; Riedle, E. *Phys. Chem. Chem. Phys.* **2009**, in press.

(46) Nosenko, Y.; Wiosna-Salyga, G.; Kunitski, M.; Petkova, I.; Singh, A.; Buma, W. J.; Thummel, R. P.; Brutschy, B.; Waluk, J. *Angew. Chem.* **2008**, *120*, 6126.

(47) Bauernschmitt, R.; Ahlrichs, R. *Chem. Phys. Lett.* **1996**, *256*, 454.

(48) Bauernschmitt, R.; Haser, M.; Treutler, O.; Ahlrichs, R. *Chem. Phys. Lett.* **1997**, *264*, 573.

(49) Furche, F.; Ahlrichs, R. *J. Chem. Phys.* **2002**, *117*, 7433.

(50) Becke, A. D. *J. Chem. Phys.* **1993**, *98*, 5648.

(51) Ahlrichs, R.; Bar, M.; Haser, M.; Horn, H.; Kolmel, C. *Chem. Phys. Lett.* **1989**, *162*, 165.

(52) Schafer, A.; Huber, C.; Ahlrichs, R. *J. Chem. Phys.* **1994**, *100*, 5829.

(53) Schafer, A.; Horn, H.; Ahlrichs, R. *J. Chem. Phys.* **1992**, *97*, 2571.

(54) Barbatti, M.; Granucci, G.; Lischka, H.; Ruckenbauer, M.; Persico, M. *NEWTON-X: a package for Newtonian dynamics close to the crossing seam, version 0.14b*, 2007, www.univie.ac.at/newtonx.

(55) Barbatti, M.; Granucci, G.; Persico, M.; Ruckenbauer, M.; Vazdar, M.; Eckert-Maksic, M.; Lischka, H. *J. Photochem. Photobiol., A* **2007**, *190*, 228.

(56) Miertus, S.; Scrocco, E.; Tomasi, J. *Chem. Phys.* **1981**, *55*, 117.

(57) Mennucci, B.; Tomasi, J. *J. Chem. Phys.* **1997**, *106*, 5151.

(58) Frisch, M. J.; Schlegel, G. W. T., H. B.; Scuseria, G. E.; Robb, M. A.; Cheeseman, J. R.; Montgomery, J. A., Jr.; Vreven, T.; Kudin, K. N.; Burant, J. C.; Millam, J. M.; Iyengar, S. S.; Tomasi, J.; Barone, V.; Mennucci, B.; Cossi, M.; Scalmani, G.; Rega, N.; Petersson, G. A.; Nakatsuji, H.; Hada, M.; Ehara, M.; Toyota, K.; Fukuda, R.; Hasegawa, J.; Ishida, M.; Nakajima, T.; Honda, Y.; Kitao, O.; Nakai, H.; Klene, M.; Li, X.; Knox, J. E.; Hratchian, H. P.; Cross, J. B.; Bakken, V.; Adamo, C.; Jaramillo, J.; Gomperts, R.; Stratmann, R. E.; Yazyev, O.; Austin, A. J.; Cammi, R.; Pomelli, C.; Ochterski, J. W.; Ayala, P. Y.; Morokuma, K.; Voth, G. A.; Salvador, P.; Dannenberg, J. J.; Zakrzewski, V. G.; Dapprich, S.; Daniels, A. D.; Strain, M. C.; Farkas, O.; Malick, D. K.; Rabuck, A. D.; Raghavachari, K.; Foresman, J. B.; Ortiz, J. V.; Cui, Q.; Baboul, A. G.; Clifford, S.; Cioslowski, J.; Stefanov, B. B.; Liu, G.; Liashenko, A.; Piskorz, P.; Komaromi, I.; Martin, R. L.; Fox, D. J.; Keith, T.; Al-Laham, M. A.; Peng, C. Y.; Nanayakkara, A.; Challacombe, M.; Gill, P. M. W.; Johnson, B.; Chen, W.; Wong, M. W.; Gonzalez, C. Pople, J. A. Gaussian, Inc.: Wallingford, CT, 2003.

(59) Kurtz, L.; Hofmann, A.; de Vivie-Riedle, R. *J. Chem. Phys.* **2001**, *114*, 6151.

(60) Karney, C. F. F. *J. Mol. Graphics Modell.* **2007**, *25*, 595.

(61) Aquino, A. J. A.; Tunega, D.; Haberhauer, G.; Gerzabek, M. H.; Lischka, H. *J. Phys. Chem. A* **2002**, *106*, 1862.

(62) Lochbrunner, S.; Wurzer, A. J.; Riedle, E. *J. Chem. Phys.* **2000**, *112*, 10699.

JP9032172